Available online at www.sciencedirect.com
ScienceDirect
Solid State Communications 146 (2008) 208–220
solid state communications
www.elsevier.com/locate/ssc

Optical magnetism and negative refraction in plasmonic metamaterials

Yaroslav A. Urzhumov, Gennady Shvets*

Department of Physics, The University of Texas at Austin, Austin, TX 78712, United States

Received 31 July 2007; accepted 16 August 2007 by the Guest Editors
Available online 12 February 2008

Abstract

In this review we describe the challenges and opportunities for creating magnetically active metamaterials in the optical part of the spectrum. The emphasis is on the sub-wavelength periodic metamaterials whose unit cell is much smaller than the optical wavelength. The conceptual differences between microwave and optical metamaterials are demonstrated. We also describe several theoretical techniques used for calculating the effective parameters of plasmonic metamaterials: the effective dielectric permittivity $\epsilon_{\text{eff}}(\omega)$ and magnetic permeability $\mu_{\text{eff}}(\omega)$. Several examples of negative permittivity and negative permeability plasmonic metamaterials are used to illustrate the theory.

PACS: 42.70.-a; 41.20.Gz; 78.67.Bf

Keywords: A. Nanostructures; C. Crystal structure and characterization; D. Optical properties

1. Introduction

A new area of electromagnetics has recently emerged: electromagnetic metamaterials. The emergence of this new field happened in response to the demand in materials with the electromagnetic properties that are not available in naturally occurring media. One of the best known properties unattainable without significant metamaterials engineering is a negative refractive index. The main challenge in making a negative index metamaterial (NIM) is that both the effective dielectric permittivity ϵ_{eff} and magnetic permeability μ_{eff} must be negative [1]. Numerous applications exist for NIMs in every spectral range, from microwave to optical. Those include "perfect" lenses, transmission lines, antennas, electromagnetic cloaking, and many others [2–5]. Recent theoretical [6,7] and experimental [8] work demonstrated that for some applications such as electromagnetic cloaking it may not even be necessary to have a negative index: just controlling the effective magnetic permeability suffices.

First realizations of NIMs were made in the microwave part of the spectrum [9]. The unit cell consisted of a metallic split-ring resonator (SRRs) [10] (responsible for the negative permeability $\mu_{\text{eff}} < 0$) and a continuous thin metal wire [11] (responsible for the negative permittivity $\epsilon_{\text{eff}} < 0$). Remarkably, even in the first microwave realizations of the NIM its unit cell was strongly sub-wavelength: $a/\lambda \approx 1/7$, where a is the lattice constant and λ is the vacuum wavelength. In fact, the condition of $a \ll \lambda$ must be satisfied in order for the effective description using ϵ_{eff} and μ_{eff} to be sensible. If the electromagnetic structure consists of larger unit cells with $a \geq \lambda/2n_d$, where n_d is the refractive index of a substrate onto which metallic elements are deposited (e.g. Duroid in some of the recent microwave experiments [8]), they cannot be described by the averaged quantities such as permittivity and permeability. It is the high λ/a ratio that distinguishes a true meta-material from its more common cousin, photonic crystal [12,13].

Developing NIMs for optical frequencies, however, has proven to be much more challenging than for microwaves. Microwave structures can be made extremely sub-wavelength using several standard microwave approaches to making a sub-wavelength resonator: enhancement of the resonator's capacitance by making its aspect ratios (e.g., ratio of the SRR's radius and gap size) high, inserting high-permittivity materials into SRR's gap, etc. These microwave techniques are briefly illustrated in Section 1.1 using a simple SRR shown in Fig. 1. Simply scaling down NIMs from microwave to optical

* Corresponding author.
E-mail address: gena@physics.utexas.edu (G. Shvets).

0038-1098/$ - see front matter © 2008 Elsevier Ltd. All rights reserved.
doi:10.1016/j.ssc.2007.08.047

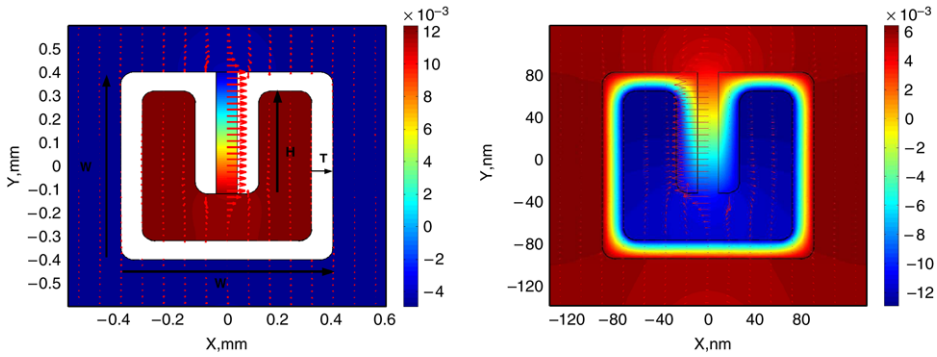

Fig. 1. Magnetic field distribution inside a lattice of split-ring resonators. Resonator parameters: periods $a_x = a_y = 1.2$ mm, ring size $W = 0.8$ mm, ring thickness $T = 80$ μm, gap height $H = 0.44$ mm, gap width $G = 80$ μm. The gap is filled with a high-permittivity dielectric $\epsilon_d = 4$. At the magnetic cutoff ($\mu_{\text{eff}} = 0$) shown here the vacuum wavelength $\lambda = 1.57$ cm.

wavelengths does not work for two reasons. First, to develop a $\lambda/10$ unit cell requires much smaller (typically, another factor 10) sub-cellular features such as metallic line widths and gaps. For $\lambda = 1$ μm that corresponds to 10 nm features which are presently too difficult to fabricate. For example, the classic SRR has been scaled down to $\lambda = 3$ μm, but further wavelength reduction using the same design paradigm seems unpractical. Second, as the metal line width approaches the typical skin depth $l_{\text{sk}} \approx 25$ nm, metal no longer behaves as an impenetrable perfect electric conductor (PEC). Optical fields penetrate into the metal, and the response of the structure becomes *plasmonic*.

These difficulties have not deterred the researchers from trying to fabricate and experimentally test magnetically-active and even negative index structures in the infrared [14–17] and even visible [18,19] spectral regions. Because fabricating intricate metallic resonators on a nanoscale is not feasible, much simpler magnetic resonances such as pairs of metallic strips or wires [14,16,17] or metallic nanoposts [18] have been used in the experiments. Unfortunately, so far there has been no success in producing *sub-wavelength* magnetically-active metamaterials in the optical range satisfying $a < \lambda/2n_d$, where n_d is the refractive index of a dielectric substrate or filler onto which magnetic materials are deposited. The reason for this is very simple [20]: in the absence of *plasmonic effects*, simple geometric resonators (such as pairs of metal strip or wires) resonate at the wavelength $\lambda \sim 2n_d L$, where L is the characteristic size of the resonator. In other words, "simple" metallic resonators are not sub-λ resonators.

Fortunately, metallic resonators can be miniaturized using *plasmonic effects* [20–23]. In the optical regime metals can no longer be described as perfect electric conductors. Instead, they are best described by a frequency-dependent plasmonic dielectric permittivity $\epsilon(\omega) \equiv \epsilon' + i\epsilon''$. For low-loss metals such as silver, $\epsilon'' \ll |\epsilon'|$ and $\epsilon' \ll -1$. Therefore, there is a significant field penetration into metallic structures that are thinner than or comparable with the skin depth $l_{\text{sk}} = \lambda/2\pi\sqrt{-\epsilon'} \approx 25$ nm. In metals $\epsilon(\omega)$ is determined by the Drude response of the free electron to the optical fields. When the kinetic energy of the oscillating free electrons becomes comparable to the energy of the electric field, one can refer to the structure as being operated in a plasmonic regime. One of the most serious issues in the plasmonic regime: as it turns out, even a small amount of losses can drastically reduce the magnetic response and prevent access to the $\mu_{\text{eff}} < 0$ regime.

Presently, the only theoretical method of characterizing plasmonic metamaterials is by carrying out fully electromagnetic scattering simulations, obtaining complex transmission (t) and reflection (r) coefficients, and then calculating the effective parameters ϵ_{eff} and μ_{eff} of the metamaterial from r and t [24,25]. Such direct approach is lacking the intuitive appeal and rigor of the earlier microwave work that provided semi-analytic expressions for both ϵ_{eff} [11] and μ_{eff} [10]. Moreover, the extracted parameters of a periodic structure exhibit various artifacts such as anti-resonances [26] that make their interpretation even less intuitive.

Recent progress has been made in rigorously calculating the quasi-static dielectric permittivity ϵ_{qs} of plasmonic nanostructures [22,23,27] exhibiting optical magnetism. In fact, the frequency dependence of $\epsilon_{\text{qs}}(\omega)$ of an *arbitrary* periodic nanostructure can be reduced to a set of several numbers [28,29] (frequencies and strengths of various electric dipole resonances) that can be obtained by solving a generalized eigenvalue equation. However, there has been a very limited progress in calculating the magnetic permittivity of such structures. Only for several specific structures has $\mu_{\text{eff}}(\omega)$ been calculated [30–32], usually under highly restrictive assumptions.

It would be highly desirable if a simple formula expressing $\mu_{\text{eff}}(\omega)$ in terms of several easily computable parameters could be derived. The increased complexity of new devices based on magnetic metamaterials [8] further highlights the need for such rapid and intuitive determination of $\mu_{\text{eff}}(\omega)$. Simply put, it is important to obtain rigorous expressions for $\mu_{\text{eff}}(\omega)$ that are similar in their form and complexity to those available for $\epsilon_{\text{qs}}(\omega)$. In addition, the formulas for $\epsilon_{\text{qs}}(\omega)$ themselves need further refinement. For example, when the size of a plasmonic nanostructures becomes a sizable fraction of the wavelength (as small as $\lambda/6$), the assumption of $\epsilon_{\text{eff}} \approx \epsilon_{\text{qs}}$ loses accuracy. One of the reasons is that the electric dipole resonances acquire a considerable electromagnetic red shift [33] that needs to be accounted for. The main objective of this paper is to derive, in the limit of $a \ll \lambda$, accurate formulas for $\epsilon_{\text{eff}}(\omega)$ and $\mu_{\text{eff}}(\omega)$.

1.1. Why is optical magnetism difficult to achieve?

Before trying to understand how one can make a sub-wavelength magnetic material in the optical part of the spectrum, it is useful to review how magnetism is accomplished in microwave metamaterials. Consider one of the most basic design elements of negative index metamaterials: split ring resonator (SRR). The particular design shown in Fig. 1 has been recently used [8] for making an invisibility cloak. For simplicity, we've simulated an infinite array of two-dimensional (infinite in the z-direction) SRRs, with all sizes given in the caption to Fig. 1. Metal resistivity has been neglected and PEC boundary conditions used at the metal surface. The non-vanishing components of the electromagnetic field are H_z, E_x, and E_y. The following eigenvalue equation has been solved:

$$-\vec{\nabla}\cdot\left(\frac{1}{\epsilon}\vec{\nabla}H_z\right)=\frac{\omega^2}{c^2}H_z, \tag{1}$$

where $\epsilon(x, y)$ is the spatially nonuniform dielectric permittivity. Finite Elements Frequency Domain (FEFD) code COMSOL Multiphysics [34] was used for solving Eq. (1).

Periodic boundary conditions have been applied to the cell boundaries. Therefore, the calculated eigenfrequency $f = \omega/2\pi = c/\lambda = 19$ GHz ($\lambda = 1.56$ cm) corresponds to the magnetic cutoff $\mu_{\text{eff}}(f_0) = 0$. Assuming that the wave is propagating in the x-direction, the dispersion relation for the entire propagation band can be computed by setting the phase-shifted boundary conditions between the $x = -a_x/2$ and $x = +a_x/2$ sides of the unit cell. In this particular case, the propagation band extends from $f = f_0$ upwards in frequency and corresponds to $\mu_{\text{eff}} \geq 0$ and $\epsilon_{\text{eff}} > 0$. The $\mu_{\text{eff}} < 0$ region is just below f_0. Because the ratio of the SRR size to wavelength is approximately 1/20, and because its magnetic response is so strong, it can be characterized as a sub-wavelength magnetic resonator.

Why is this structure subwavelength? The natural resonance frequency of a resonator scales as $1/\sqrt{L_R C_R}$. Therefore, its size can be reduced from its "natural" $\lambda/2$ value by either increasing its inductance L_R or capacitance C_R. For this particular design the largest increase comes from the capacitance which is increased by a factor $\epsilon_d H/G \approx 36$. Note that both the narrow gap and high permittivity of the dielectric placed in the gap enhance the capacitance and reduce the resonant frequency. The role of the dielectric filling is verified by an additional numerical simulation (not shown) in which the $\epsilon_d = 4$ dielectric filler is removed from the gap. The resonant frequency increases by a factor 1.8 confirming that most of the capacitance comes from the gap region. Note that at the resonant frequency $L_R\langle I^2\rangle = \langle Q^2\rangle/C_R$, the average electric and magnetic energies are equal to each other. This intuitive result is confirmed by the numerical simulations. The fact that the average magnetic energy constitutes a significant fraction of the total energy (one-half) explains the strong magnetic response of the structure. The results of this dissipation-free simulation are not significantly affected by the finite metallic losses because microwaves penetrate by only a fraction of a micron into a typical metal (e.g., 0.45 μm into copper).

We now investigate if this structure can be naturally scaled down to optical wavelengths. Because high-ϵ_d dielectrics are not available at the optical frequencies, it is assumed that the SRR's gap is air-filled. Instead of using PEC boundary conditions at the metal surface, metal is modelled as a lossless negative-ϵ dielectric with $\epsilon(\omega)$ taken from the standard tables [35]. By scanning the value of the plasmonic ϵ (physically equivalent to scanning the frequency), we have calculated the corresponding size of the SRR that has the same geometric proportions as the one shown in Fig. 1. Losses have been neglected for this calculation: $\epsilon \equiv \epsilon'$. Nontrivial solutions of Eq. (1) corresponding to the magnetic cutoff were found only for $\epsilon < \epsilon_{\text{res}} \equiv -330$ corresponding to $\lambda > \lambda_{\text{res}} \equiv 3$ μm for silver. As will be shown below, ϵ_{res} corresponds to the *electrostatic resonance* of an SRR. The electrostatic potential ϕ corresponding to the electrostatic resonance and the corresponding electric field $\vec{E} = -\nabla\phi$ are shown in Fig. 2(a). Magnetic field distribution for $\lambda = 3.44$ μm is presented in Fig. 1. Clearly, magnetic field penetrates deep into the metal. This specific wavelength has been chosen because for $\lambda = 3.44$ μm the ratio of the wavelength to the SRR's width is the same as for the microwave design: 1/20. One may be tempted to assume that we've demonstrated a successful down-scaling (by a factor 4400) of a NIM from microwave to optical frequencies, and that there are no conceptual differences between the $\lambda = 1.56$ cm and $\lambda = 3.44$ μm. To see why this is not the case, consider the implications of the plasmonic ϵ of metals at optical frequencies.

For simplicity assume a collisionless Drude model for metal: $\epsilon(\omega) = \epsilon_b - \omega_p^2/\omega(\omega + i\gamma)$ with $\gamma = 0$. Then the total energy density

$$\begin{aligned} U_{\text{tot}} &= \int_{V_m+V_v} \mathrm{d}^2x \left(\frac{H_z^2}{8\pi} + \frac{\vec{E}^2}{8\pi}\frac{\partial(\omega\epsilon)}{\partial\omega}\right) \\ &= \int_{V_v} \mathrm{d}^2x \frac{\vec{E}^2}{8\pi} + \epsilon_b \int_{V_m} \mathrm{d}^2x \frac{\vec{E}^2}{8\pi} + \frac{\omega_p^2}{\omega^2}\int_{V_m} \mathrm{d}^2x \frac{\vec{E}^2}{8\pi} \\ &\quad + \int_{V_m+V_v} \mathrm{d}^2x \frac{H_z^2}{8\pi}, \end{aligned} \tag{2}$$

where V_v and V_m are the vacuum and metallic volumes, respectively. The physical meaning of the four terms in Eq. (2) is as follows: the first two terms represent the energy of the electric field U_E, the third one represents the kinetic energy U_k of plasma electrons, and the fourth one represents the magnetic energy U_m. Because both the kinetic and magnetic energies (with $H_z^2 = c^2/\omega^2|\vec{\nabla}_\perp \times \vec{E}|^2$) scale as ω^{-2}, these two terms can be grouped into $U_L = U_m + U_k$. Again, at the resonance the "capacitive" energy U_E matches the "inductive" energy U_L. For the most relevant cases of $|\epsilon| \gg 1$ the following rules can be established for plasmonic structures: (a) most of the capacitive energy U_E resides in the vacuum region (outside of the plasmonic material); (b) most of the magnetic energy U_m also resides in the vacuum region. Of course, the same is true for the microwave structures. The main difference between the two types of structures comes from the kinetic energy U_k present in plasmonic but absent from microwave structures.

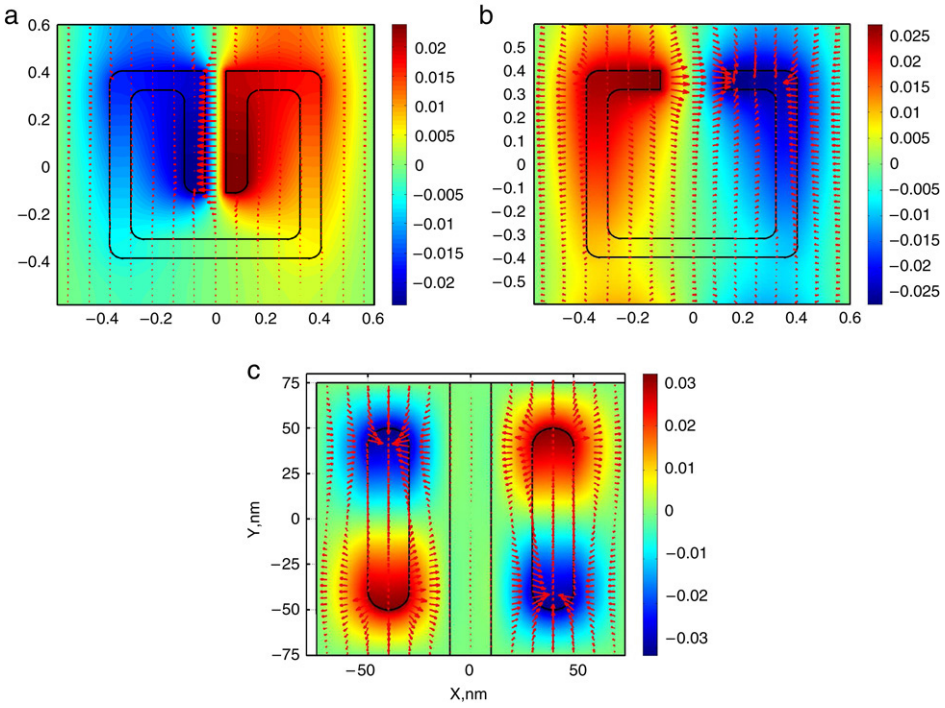

Fig. 2. Potential distribution ϕ inside a lattice of (a) split-ring resonators (SRRs), (b) split rings (SRs), and (c) metal strips separated by a metal film corresponding to electrostatic resonances responsible for the magnetic response. Arrows: $\vec{E} = -\nabla\phi$. Electrostatic resonances occur at (a) $\epsilon_{\rm res} \equiv -330$ ($\lambda = 3$ μm) for SRR, (b) $\epsilon_{\rm res} \equiv -82$ ($\lambda = 1.5$ μm) for SR, and (c) $\epsilon_{\rm res} \equiv -8.8$ ($\lambda = 0.5$ μm) assuming that the plasmonic material is silver.

It is instructive to compare the values of U_E, U_m, and U_k for the plasmonic structure. From the results of the numerical simulation shown in Fig. 1(b) it is found that $U_E = 0.5U_{\rm tot}$, $U_k = 0.32U_t$, and $U_m = 0.18U_t$. As noted earlier, for the microwave SRR $U_E = U_m = 0.5U_t$. Therefore, the distinction between the scaled-down plasmonic structure and its microwave counterpart is the contribution of the kinetic energy U_k of the Drude electrons vs that of the magnetic energy U_m. In the present example, U_k exceeds U_m by almost a factor 2. Thus it is fair to say that the present structure operates in a stronly plasmonic regime. This is quite remarkable, given that the operating wavelength $\lambda = 3.44$ μm is fairly long. To quantify the plasmonic effects in a magnetic structure, we introduce the plasmonic parameter $T_p = U_k/U_m$. The structure can be said to operate in a strongly plasmonic regime when $T > 1$. Plasmonic SRR can be made even more sub-wavelength by reducing the operating wavelength to $\lambda = \lambda_{\rm res}$. Of course, this happens at the expense of the magnetic energy: the plasmonic parameter T_p diverges as the structure shrinks and the operating wavelength approaches that of the electrostatic resonance. At the electrostatic resonance $T_p = \infty$ and $U_E = U_k$. The analogy between the plasmonic energy and inductance energy has been suggested earlier [36].

The importance of having a reasonably small plasmonic parameter for making a magnetic resonator becomes apparent when losses are taken into account. Achieving $\mu_{\rm eff} = 0$ (qualitative threshold for a strong magnetic response) sets a threshold for the magnetic energy U_m in the resonator. The total energy $U_{\rm tot} = 2(1 + T_p)U_m$ increases with T_p. This reduces the group velocity of the propagating mode, with the effect of narrowing the propagation band. Even small losses tend to destroy such bands. To get a qualitative estimate of the role of resistive losses we assume a finite γ in the Drude model. The group velocity can be roughly estimated as $v_g/c \sim U_m/U_t$. The propagation band is assumed to be destroyed by losses if the transit time across a single cell is longer than the decay time γ^{-1}, or $a_x/v_g > \gamma^{-1}$. This results in the following condition for achieving optical magnetism in a lossy system:

$$\frac{\gamma}{\omega} \approx \frac{\epsilon''}{\epsilon'} < \left[\frac{\omega a_x}{c}\left(1 + T_p\right)\right]^{-1}. \tag{3}$$

This condition is trivially satisfied for any sub-wavelength structure as long as T_p is of order unity. It becomes increasingly difficult to satisfy for the structures operated in a strongly plasmonic regime as will be shown below. Note that in the absence of losses strong magnetic response of a sub-wavelength SRR can be achieved for any $\lambda > \lambda_{\rm res}$.

Several instructive conclusions can be drawn from the above examples of the large (microwave) and small (mid-infrared) rings. First, for given geometry of the unit cell there exists the shortest wavelength $\lambda_{\rm res}$ for which a strong magnetic response is expected. This wavelength corresponds to the electrostatic resonance of the structure, and for the SRR geometry shown in Fig. 1 $\lambda_{\rm res} = 3$ μm. Strong optical response can be obtained for any $\lambda > \lambda_{\rm res}$, with the actual dimensions of the ring adjusted accordingly. The positive result here is that even for a very sub-wavelength ring ($\lambda/20$) the plasmonic parameter $T_p \approx 2$ is modest and, therefore, finite losses are not affecting the magnetic response. The negative result is that the standard SRR design cannot be used for obtaining magnetic response

for visible/near-infrared frequencies because the electrostatic resonance occurs in mid-infrared.

The rule of thumb is that the more elaborate is the design of the plasmonic structure, the longer is the wavelength of the electrostatic resonance. For example, for a simplified version of the SRR (no vertical capacitor-forming strips, similar to the one used earlier [37]) it is found that the electrostatic resonance occurs at $\lambda_{\text{res}} = 1.5$ μm (corresponding $\epsilon_{\text{res}} = -82$). The electrostatic potential ϕ and the corresponding electric field $\vec{E} = -\nabla\phi$ are shown in Fig. 2(b). Using a typical dielectric substrate or a filler with $\epsilon_d = 2.25$ would reduce the resonant permittivity to $\epsilon_{\text{res}} = -186$ (corresponding to $\lambda_{\text{res}} = 2.25$ μm for Ag). At the same time, this design simplification comes at a cost: for very long wavelengths (microwave) such split ring (SR) is only moderately sub-wavelength, with $\lambda/W = 5.2$. Again, using a filler with $\epsilon_d = 2.25$ would result in $\lambda/W = 7.8$. If a more sub-wavelength resonator is required, one needs to operate in the vicinity of λ_{res}. The drawback of operating too close to λ_{res} is a high plasmonic parameter T_p and, therefore, susceptibility to resistive losses.

Of course, the structure can be simplified even further: from a split ring to a pair of metal strips [15,20] or a pair of metal strips separated by a thin metal film [27]. The advantage of this structural simplification is that the magnetically-active plasmonic resonance is pushed even further into the visible/near-infrared part of the spectrum: $\lambda_{\text{res}} = 0.5$ μm without a dielectric filler and $\lambda_{\text{res}} = 0.7$ μm with the $\epsilon_d = 2.25$ filler. The potential distribution for the Strip Pair-One Film (SPOF) structure is shown in Fig. 2(c). Because of the promise of the SPOF for NIM development, we have scaled the structure in nanometers. Of course, the results of electrostatic simulations can be plotted with an arbitrary spatial scale (as was done in Fig. 2((a), (b)) because there is no spatial scale in electrostatics. In the PEC limit (long wavelength) the ratio of the wavelength to period was found to be $\lambda/a_x = 1.85$ at the magnetic cutoff for the SPOF structure without a filler, and $\lambda/a_x = 2.8$ with the $\epsilon_d = 2.25$ filler. Therefore, the SPOF structure presents a unique opportunity for developing a strongly sub-wavelength ($\lambda/10 - \lambda/6$) optical (visible to near-IR) NIM. As was recently shown [27], the addition of a thin film modifies the electric response of the double-strip structure and turns this magnetically-active metamaterial into a true sub-wavelength ($a_x = \lambda/6$) NIM. The simple qualitative remarks presented above explain why. Note that no optical NIM with the cell size smaller that $\lambda/2.5$ has ever been experimentally demonstrated [14–17].

We summarize this section by noting that optical magnetic resonators are conceptually very different from their microwave counterparts. Intricate designs of microwave resonators (such as SRRs) are simply inappropriate for optical frequencies because they lose their strong response for $\lambda < \lambda_{\text{res}}$. This is a *rigorous quantitative result*: for a given resonator geometry, there is no strong magnetic response for the wavelengths shorter than the one corresponding to the electrostatic resonance. λ_{res} enters the electrostatic theory parametrically, through the dependence of the metal's dielectric permittivity: $\epsilon(\lambda) < \epsilon_{\text{res}} \equiv \epsilon(\lambda_{\text{res}})$ is necessary for the strong response. Because intricate SRR designs correspond to extremely large negative values of ϵ_{res}, they do not exhibit a strong magnetic response in the visible/near-infrared parts of the spectrum. Therefore, the transition from SRRs (see Fig. 2(a)) to simple pairs of strips (see Fig. 2(c)) is not just a matter of fabricational convenience: it is physically necessary for making optical NIMs. The price one pays for using the simplified structures is that they are no longer sub-wavelength for $\lambda \gg \lambda_{\text{res}}$. Therefore, one is forced to operate close to λ_{res}. The price for that is the significant plasmonic effects that enhance the plasmonic parameter T_p and make the bandwidth of the magnetic response very narrow. That makes these near-resonant structures highly susceptible to losses according to Eq. (3). Thus, plasmonic effects play two roles in optical magnetism. Their positive role is in turning simple metallic structures into sub-wavelength resonators. Their negative role is in enhancing the effects of losses.

Thus, the role of an optical NIM designer is to choose a structure that (a) has a λ_{res} in the visble/mid-IR, and (b) is sufficiently sub-wavelength in the PEC limit (long λ) that the structure does not need to be operated too close to λ_{res}. The electrostatic resonance at λ_{res} is the natural starting point for computing the optical response of the sub-wavelength metamaterial. In the rest of the paper we present an analytic perturbation theory of the electric and magnetic responses of a plasmonic nanostructure in the optical frequency range that uses the electrostatic resonances as the expansion set. Section 2 describes several techniques of calculating the effective dielectric permittivity $\epsilon_{\text{eff}}(\omega) \approx \epsilon_{\text{qs}}(\omega)$ in the quasi-static regime. Section 3 describes the quasi-static calculation of the effective magnetic permeability $\mu_{\text{eff}}(\omega)$.

2. Effective quasi-static dielectric permittivity of a plasmonic metamaterial

Several theoretical techniques are available for calculating $\epsilon_{\text{qs}}(\omega)$ of plasmonic nanostructures: (a) the "capacitor" approach described in Section 2.1: voltage is imposed across the unit cell of a structure, and the effective capacitance is evaluated; (b) the method of homogenizing electrostatic equations using a multi-scale expansion described in Section 2.2, with the two independent spatial variables: the intra-cell (small scale) variable $\vec{\xi}$ and the inter-cell (large scale) variable $\vec{X}$; (c) and the method of electrostatic eigenvalues, and its extension to plasmonic structures with continuous plasmonic phase described in Section 2.3.

2.1. The "capacitor" model

The most simple and intuitive method of introducing the effective dielectric permittivity of a complex periodic plasmonic metamaterial is to imagine what happens when a single cell of such structure is immersed in a uniform electric field. For simplicity, all calculations in Section 2 will be limited to a two-dimensional case, i.e. the system is assumed uniform along the z-axis; generalizations to three dimensions are straightforward. To further simplify our calculations, it

will be assumed that the unit cell is a rectangle of the size $a_x \times a_y$ in the xy plane: $-a_x/2 < x < a_x/2$ and $-a_y/2 < y < a_y/2$. The unit cell is assumed to consist of a plasmonic inclusion with a complex frequency-dependent dielectric permittivity $\epsilon(\omega)$ embedded into a dielectric host with the dielectric permittivity ϵ_d. The plasmonic inclusion may intersect the unit cell's boundary. We assume that the structure has an inversion symmetry and two axes of reflection (x and y). In that case the effective permittivity tensor is diagonal: $\epsilon_{\rm qs} = \mathrm{diag}(\epsilon_{\rm qs}^{xx}, \epsilon_{\rm qs}^{yy})$.

Applying a constant electric field $\vec{E}_0 = \vec{e}_x E_{0x} + \vec{e}_y E_{0y}$ is equivalent to solving the Poisson equation for the potential $\phi \equiv \phi_{\vec{E}_0}$:

$$\vec{\nabla} \cdot (\epsilon \vec{\nabla} \phi) = 0 \tag{4}$$

on a rectangular domain $ABCD$ (where AB and CD are parallel to y, BC and AD are parallel to x). The external electric field $\vec{E}_0$ determines the boundary conditions satisfied by ϕ: (a) $\phi(x + a_x, y) = \phi(x, y) - E_{0x} a_x$, where (x, y) belongs to AB, and (b) $\phi(x, y + a_y) = \phi(x, y) - E_{0y} a_y$, where (x, y) belongs to AD. We now view the unit cell of a metamaterial as a tiny capacitor immersed in a uniform electric field which is created by the voltage applied between its plates. For calculating $\epsilon_{\rm qs}^{xx}$ assume that the voltage $V_0 = E_{0x} a_x$ is applied between its sides AB and CD, and that $E_{0y} = 0$. From the potential distribution $\phi(x, y)$ the required surface charge density on the "capacitor plate" AB is $\sigma(y) = (\vec{n} \cdot \vec{D}) = -\epsilon_d \partial_x \phi(x = -a_x/2, y)$. The total charge (per unit length in z) on the capacitor is $Q = \int_{-a_y/2}^{+a_y/2} \mathrm{d}y \sigma(y)$. The opposite capacitor plate CD is oppositely charged. The unit length capacitance of this capacitor, $C \equiv \epsilon_{\rm qs}^{xx} a_y / a_x$ is thus given by $C = Q/V_0$, or

$$\begin{aligned} \epsilon_{\rm qs}^{xx} &= -\frac{\epsilon_d a_x}{E_0 a_y} \int_{-a_y/2}^{+a_y/2} \mathrm{d}y \partial_x \phi(x = -a_x/2, y) \\ &\equiv \frac{a_y^{-1} \int_{-a_y/2}^{a_y/2} \mathrm{d}y D_x(x = -a_x/2, y)}{a_x^{-1} \int_{-a_x/2}^{a_x/2} \mathrm{d}x E_x(x, y = -a_y/2)}. \end{aligned} \tag{5}$$

The $\epsilon_{\rm qs}^{yy}$ component is determined similarly by applying the voltage $V_0 = E_{0y} a_y$ between the capacitor plates AD and BC. Both $\epsilon_{\rm qs}^{xx}$ and $\epsilon_{\rm qs}^{yy}$ depend parametrically on the frequency ω because of the $\epsilon(\omega)$ dependence of the plasmonic permittivity. Therefore, extracting the frequency-dependent components of $\epsilon_{\rm qs}$ tensor involves scanning the frequency ω, repeatedly solving (4) with the described boundary conditions, and applying the capacitance-based definition of $\epsilon_{\rm qs}$ given by Eq. (5). We refer to this technique of extracting the electrostatic $\epsilon_{\rm eff}$-tensor as the "frequency scan" technique. As it turns out, there is a faster and more physically appealing approach to calculating $\epsilon_{\rm eff}^{ij}(\omega)$, described in Section 2.3. Note that the definition of the effective permittivity given by Eq. (5) is equivalent to the one introduced earlier by Pendry et al. in [10] which was derived [38] from the integral form of Maxwell's equations.

The capacitor model can be shown to be equivalent to another intuitive definition of $\epsilon_{\rm qs}$ based on the dipole moment density. The total dipole moment of a unit cell $\vec{p} = \int \mathrm{d}x\mathrm{d}y \vec{P}$ (where $\vec{P} = \frac{\epsilon - 1}{4\pi} \vec{E}$ is the polarization density) is linearly proportional to the external electric field $\vec{E}_0$. In a homogeneous medium with anisotropic $p_i = \frac{1}{4\pi} \left(\epsilon_{\rm qs}^{ij} - \delta^{ij} \right) E_{0j} a_x a_y$, where $\epsilon_{\rm qs}^{ij}$ is the effective permittivity tensor. Therefore, $\epsilon_{\rm qs}$ can be defined by requiring that

$$a_x a_y (\epsilon_{\rm qs}^{ij} - \delta^{ij}) E_{0j} \equiv \int \mathrm{d}x\mathrm{d}y (\epsilon - 1) E_i. \tag{6}$$

Because $\int \mathrm{d}x\mathrm{d}y E_i = a_x a_y E_{0i}$, this *dipole density* definition of $\epsilon_{\rm qs}$ simplifies to

$$a_x a_y \epsilon_{\rm qs}^{ij} E_{0j}^{(k)} \equiv \int \mathrm{d}x\mathrm{d}y D_i^{(k)} = \int \mathrm{d}x\mathrm{d}y \epsilon E_i^{(k)}, \tag{7}$$

where the external field $E_{0j}^{(k)} \equiv E_0 \delta_{jk}$ applied to the unit cell produces the total internal field $\vec{E}^{(k)}$, and $k = 1, 2$. The internal electric fields are computed by solving Eq. (4) subject to its $\vec{E}_0^{(k)}$-dependent boundary conditions. Eq. (7) is equivalent to the capacitance-based definitions of $\epsilon_{\rm qs}$ given by Eq. (5). Owing to an identity $\int \mathrm{d}x\mathrm{d}y D_i = \oint \mathrm{d}s x_i (\vec{D} \cdot \vec{n})$, where $\vec{n}$ is the unit normal to the closed contour of integration (unit cell boundary), Eq. (7) is expressed through a contour integral of the first kind:

$$\epsilon_{\rm qs}^{ij} E_{0j}^{(k)} = \frac{1}{a_x a_y} \oint \mathrm{d}s x_i (\vec{D}^{(k)} \cdot \vec{n}). \tag{8}$$

This contour integral indeed reduces to the surface charge on the capacitor plates. For example, for x-polarized external field ($k = 1$) we obtain $\oint \mathrm{d}s x (\vec{D} \cdot \vec{n}) = (-a_x/2)(-Q) + (a_x/2) Q = a_x Q$, thereby completing the proof of equivalence between definitions (5) and (6). All formulas of this Section can be generalized to 3D. Also, note that Eq. (8) can be used for determining *all* (diagonal and off-diagonal) elements of tensor $\epsilon_{\rm qs}$ of an arbitrary nanostructure (with or without inversion symmetry of a unit cell), because the number of unknown components of $\epsilon_{\rm qs}$ is equal to the number of equations.

2.2. Effective medium description through electrostatic homogenization

While the capacitance model developed in Section 2.1 is simple and intuitive, it needs to be justified in the context of the rigorous homogenization theory. In this section we review a multi-scale approach [39,40] to calculating the effective permittivity of a metamaterial and show its equivalence with the capacitance model. Also known as the homogenization theory of differential operators with periodic coefficients [39,40], it is the most vigorous approach to homogenizing a periodic metamaterial with a unit cell size a being much smaller than that of the typical variation scale Λ of the dominant electrostatic potential Φ. As in the previous sections, the key assumption leading to the electrostatic approximation is that $\omega a/c \ll \omega \Lambda/c \ll 1$. Under this set of assumptions, the frequency ω enters only as a parameter determining the plasmonic dielectric permittivity $\epsilon(\omega)$. The basis of the method is the two-scale expansion. Let $\vec{X}$ be the macroscopic coordinates enumerating

the cells (large spatial scale Λ), and $\vec{\xi}$ the local coordinates inside the unit cell (small spatial scale a). The potential $\phi(\vec{X},\vec{\xi})$ and the local permittivity $\epsilon(\vec{\xi})$ are periodic in $\vec{\xi}$; the latter can be restricted to one cell.

Using $\tau = a/\Lambda$ as the small parameter, we expand $\phi(x) = \phi_0(X,\xi) + \tau\phi_1(X,\xi) + \tau^2\phi_2(X,\xi) + O(\tau^3)$ and use $\nabla_x = \nabla_\xi + \tau\nabla_X$ to solve the Laplace equation $\nabla_x\epsilon(x)\nabla_x\phi(x) = 0$ order-by-order in τ. The goal of homogenization theory is to show that there exists a macroscopic potential $\phi_{\text{macro}}(X)$ that obeys Laplace–Poisson equation in a certain homogeneous, possibly anisotropic, medium. In doing so, both the rigorous definitions of $\phi_{\text{macro}}(X)$ and $\epsilon^{ij}_{\text{eff}}$ are discovered. This goal is achieved by expanding Poisson equation in powers of τ. Terms with different powers of τ must vanish independently, resulting in three equations:

$$\nabla_\xi\epsilon(\xi)\nabla_\xi\phi_0(X,\xi) = 0, \tag{9}$$

$$\nabla_\xi\epsilon(\xi)\nabla_\xi\phi_1(X,\xi) = -\left(\nabla_\xi\epsilon(\xi) + \epsilon(\xi)\nabla_\xi\right)\nabla_X\phi_0(X,\xi), \tag{10}$$

$$\nabla_X\epsilon(\xi)\nabla_X\phi_0(X,\xi) + \left(\epsilon(\xi)\nabla_\xi + \nabla_\xi\epsilon(\xi)\right)\nabla_X\phi_1(X,\xi) + \nabla_\xi\epsilon(\xi)\nabla_\xi\phi_2(X,\xi) = 0. \tag{11}$$

Eq. (9) is satisfied by $\phi_0(X,\xi) \equiv \phi_0(X)$, where the role of the macroscopic potential is played by $\phi_0(X)$. Next, $\phi_1(X,\xi)$ is expressed through the macroscopic gradients of ϕ_0:

$$\phi_1(X,\xi) = -\frac{\partial\phi_0(X)}{\partial X_i}\phi^{(i)}_{\text{sc}}(\xi), \tag{12}$$

where $\phi^{(i)}_{\text{sc}}(\xi)$ ($i = 1,2$ in 2D) are periodic basis functions satisfying the local Poisson equation:

$$\vec{\nabla}_\xi\cdot\epsilon(\xi)\vec{\nabla}_\xi\phi^{(i)}_{\text{sc}}(\xi) = \left(\vec{\nabla}_\xi\epsilon(\xi)\right)\cdot\vec{e}_i, \tag{13}$$

where $\vec{e}_i$ is the ith basis vector of Cartesian coordinate system. Note that the periodic potentials $\phi^{(i)}_{\text{sc}}$ are linearly related to the $\phi_{\vec{E}_0}$ defined by Eq. (4) through $\phi_{\vec{E}_0} \equiv \left(E_{0i}\phi^{(i)}_{\text{sc}}(\xi) - \vec{E}_0\cdot\vec{\xi}\right)/|\vec{E}_0|$. The difference between Eqs. (13) and (4) is that the macroscopic electric field $\vec{E}_0 \equiv -\vec{\nabla}_X\phi_0$ is explicitly included in the rhs in (13) and embedded in the boundary conditions in (4).

Finally, the macroscopic equation for $\phi_0(X)$ is obtained by substituting ϕ_1 from Eq. (12) into Eq. (11) and averaging over the local variable ξ: $\nabla_{X_i}\epsilon^{ij}_{\text{qs}}\nabla_{X_j}\phi_{\text{macro}}(X) = 0$, where $\phi_{\text{macro}}(X) \equiv \phi_0(X) \equiv \langle\phi(X,\xi)\rangle$ and

$$\epsilon^{ij}_{\text{qs}} = \langle\epsilon(\xi)\delta_{ij} - \epsilon(\xi)\nabla_{\xi_i}\phi^{(j)}_{\text{sc}}(\xi)\rangle \equiv \langle\epsilon(\xi)\nabla_{\xi_i}(\xi_j - \phi^{(j)}_{\text{sc}}(\xi))\rangle; \tag{14}$$

angle brackets denote averaging over the unit cell, $\langle F\rangle \equiv \int F\mathrm{d}^2\xi/\int\mathrm{d}^2\xi$. It can be shown that this definition of ϵ_{qs} is equivalent to the one obtained from the capacitor model. Indeed, note that $\vec{E}^{(i)}(\xi) = \vec{\nabla}_\xi(-\phi^{(i)}_{\text{sc}}(\xi) + \xi_i)$ is the total electric field excited by external electric field $\vec{E}_0 = \vec{e}_i$ with the unit amplitude. Therefore, Eq. (14) is equivalent to $\epsilon^{ij}_{\text{qs}} = \langle\epsilon(\xi)E^{(j)}_i(\xi)\rangle$, in exact agreement with Eq. (7).

2.3. Eigenvalue expansion approach

The frequency scan technique described in Section 2.1 is a simple yet time consuming approach to calculating the quasistatic response of sub-wavelength metamaterials. Electrostatic eigenvalue (EE) approach [22,28,41] enables calculate this response for a wide range of frequencies by evaluating the position and strength of the electric dipole active plasmonic resonances in that range. As we shall see from examples below, there are only a few eigenmodes that contribute to ϵ_{qs}, making the EE approach extremely efficient. Additional theoretical insights (such as the Hermitian nature of ϵ_{qs} that is not evident from Eq. (7)) can be gained from the EE approach. In addition to reviewing some of the known facts about the EE approach [28,29,41] to calculating ϵ_{qs}, we extend the original theory of plasmon resonances to include plasmonic metamaterials with continuous plasmonic phase. Such structures have become increasingly important in the field of negative index materials (NIMs) since the introduction of the so-called *fishnet* structure [14,17], as well as the SPOF structure [27].

One way of obtaining eigenvalue expansions is the *generalized eigenvalue differential equation* (GEDE) [22,41]. Another, essentially equivalent, method is based on a surface integral eigenvalue equation [33,42]. The steps of the GEDE approach are briefly described here, with the details appearing elsewhere [22,23]. We assume that a periodic nanostructure consists of two dielectric, non-magnetic materials: one with a frequency-dependent permittivity $\epsilon(\omega) < 0$ and another with permittivity ϵ_d. Local permittivity of such a structure is $\epsilon(\vec{r},\omega) = \epsilon_d\left[1 - \frac{1}{s(\omega)}\theta(\vec{r})\right]$, where $\theta(\vec{r}) = 1$ inside the plasmonic material and $\theta(\vec{r}) = 0$ elsewhere, and $s(\omega) = (1-\epsilon(\omega)/\epsilon_d)^{-1}$ is the frequency label.

First, the GEDE

$$\vec{\nabla}\cdot\left[\theta(\vec{r})\vec{\nabla}\phi_n\right] = s_n\nabla^2\phi_n \tag{15}$$

is solved for the real eigenvalues s_n. Spectral properties of the GEDE are discussed in detail in [29,41] and references therein. Second, the solution of Eq. (4) is expressed as an eigenmode expansion [41]

$$\phi(\vec{r}) = \phi_0(\vec{r}) + \sum_n \frac{s_n}{s(\omega)-s_n}\frac{(\phi_n,\phi_0)}{(\phi_n,\phi_n)}\phi_n(\vec{r}), \tag{16}$$

where the scalar product is defined as $(\phi,\psi) = \int\mathrm{d}x\mathrm{d}y\theta\vec{\nabla}\phi^*\cdot\vec{\nabla}\psi$, and $\phi_0 = -E_0x$ represents x-polarized external field. Third, the quasistatic permittivity is calculated by substituting $\phi(\vec{r})$ from Eq. (16) into any of the equivalent definitions of ϵ_{qs}. For example, the dipole moment definition (6) leads to the following analytical expression for ϵ_{qs}:

$$\epsilon^{ij}_{\text{qs}}(\omega) = \epsilon_d\left(\delta_{ij} - \frac{f^{ij}_0}{s(\omega)} - \sum_{n>0}\frac{f^{ij}_n}{s(\omega)-s_n}\right), \tag{17}$$

where $f^{ij}_n = A^{-1}(\phi_n,x_i)(\phi_n,x_j)/(\phi_n,\phi_n)$ are the electric dipole strengths of the nth resonance,

$$f_0^{ij} = (A_p/A)\delta_{ij} - \sum_{n>0} f_n^{ij} \tag{18}$$

is the measure of the electric response of the continuous plasma phase, and $A_p = \int \mathrm{d}x\mathrm{d}y\theta(\vec{r})$ is the area of the plasmonic phase contained within the area $A = a_x a_y$ of a unit cell. From the expression for f_n^{ij} we note that only dipole-active resonances having a non-vanishing dipole moment (ϕ_n, x_j) contribute to the dielectric permittivity. Examples of such resonances are shown in Fig. 2((a),(b)) for the SRR and SR. But the electrostatic resonance of the SPOF structure shown in Fig. 2(c) is not dipole-active. It does not contribute to ϵ_{qs} but, as will be shown in Section 3.1, contributes to the magnetic permeability.

Application of the equivalent capacitance definition given by Eq. (8) leads to the same Eq. (17) with the same f_n^{ij}. However f_0^{ij} is obtained in a different (and more instructive) form:

$$f_0^{ij} = q^{ij} - \frac{1}{A}\sum_n \frac{(\phi_n, x_j)}{(\phi_n, \phi_n)} \oint \mathrm{d}s\theta x_i \frac{\partial \phi_n}{\partial n}, \tag{19}$$

where $\partial/\partial n$ is the normal derivative, $q^{ij} = \frac{1}{A}\oint \mathrm{d}s\theta x_i \frac{\partial x_j}{\partial n}$, and contour integration is carried out over the boundary of a unit cell. Note that, if there is no continuous plasmonic phase inside the unit cell of a nanostructure, its boundaries can be chosen such that they are not intersected by the plasmonic inclusion and, therefore, $f_0^{ij} \equiv 0$. Combining Eqs. (18) and (19) results in a generalized sum rule for plasmonic oscillators in nanostructures that contain a continuous plasmonic phase.

To illustrate this method, we chose the two-dimensional SPOF [27] shown in Fig. 2(c). The real and imaginary parts of the yy-component of ϵ_{qs} corresponding to electric field along the film are plotted as dashed and dash-dotted lines on Fig. 3, respectively. The green and black dashed lines show $\mathrm{Re}\,\epsilon_{\mathrm{qs}}^{yy}$ with and without the retardation correction to the frequency of the plasmon resonances. It is generally known [33] that frequencies of the optical resonances of finite-sized nanoparticles (with the typical spatial dimension w) are red-shifted from their electrostatic values because of the retardation effects proportional to $\eta^2 \equiv \omega^2 w^2/c^2$. As shown in Section 3.2, these shifts can be expressed as corrections to the frequency labels s_n: $s_n = s_n^{(0)} + s_n^{(2)}$, where $s_n^{(0)}$ are the electrostatic resonances and $s_n^{(2)}$ are the retardation corrections computed in Section 3.2. To obtain any meaningful comparison between the electromagnetically-extracted values of ϵ_{eff} and the electrostatic ϵ_{qs}, these corrections must be included even for the structures as small as $\lambda/10$.

In the chosen range of frequencies, there are only two dipolar resonances that contribute to ϵ^{yy}; quasistatic curves in Fig. 3 are computed from the Eq. (17) with the following numerical coefficients: conduction pole residue $f_0^{yy} = 0.043$, electric resonance strengths $f_1^{yy} = 0.0045$, $f_2^{yy} = 0.0005$, and pole positions $s_n = s_n^{(0)} + s_n^{(2)}$ with $s_1^{(0)} = 0.0426$, $s_2^{(0)} = 0.1630$ and $s_1^{(2)} = -0.007$, $s_2^{(2)} = -0.004$. The other component of ϵ_{qs} has no resonances between $\lambda = 500 - 800$ nm and remains approximately constant, $\epsilon_{\mathrm{qs}}^{xx} \approx 1.2$ in the frequency range covered by Fig. 3. Quasistatic calculations of $\epsilon_{\mathrm{qs}}^{yy}$ are

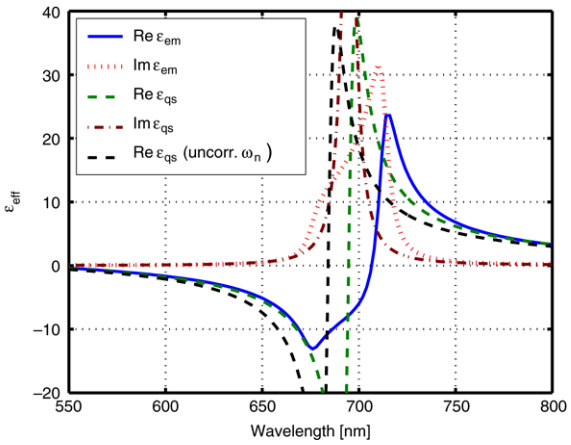

Fig. 3. (Color online) Effective dielectric permittivity $\epsilon_{\mathrm{eff}}^{yy}$ of the SPOF structure (with the film in yz plane) calculated using two methods: electromagnetic scattering through a single layer (solid and dotted curves), and quasi-static formula (17) (dashed and dash-dotted). Red-shifted green dashed curve differs from the black dashed one by the frequency shift (32) discussed in Section 3.2. Structure parameters: periods $a_x = 100$ nm, $a_y = 75$ nm, strip width $w = 50$ nm, strip thickness $t_s = 15$ nm, film thickness $d_f = 5$ nm, strip separation in a pair $h = 15$ nm; plasmonic component: silver (Drude model); immersion medium: $\epsilon_d = 1$.

compared with the $\epsilon_{\mathrm{em}} \equiv \epsilon_{\mathrm{eff}}$ extracted from the first-principles electromagnetic scattering simulations [24–26] of a single layer of SPOF. Electromagnetic simulations are performed using FEFD method implemented in the software package COMSOL Multiphysics [34]. Overall, agreement between ϵ_{em} and ϵ_{qs} is very good everywhere except near the strong absorption line associated with electric resonance at $\approx$ 700 nm. Inside that band (680–720 nm) the shape of ϵ_{em} strongly deviates from Lorentzian. We speculate that this irregularity of ϵ_{em} is related to the large phase shift per cell $\theta \equiv k_x a_x = \mathrm{Re}\,[\sqrt{\epsilon_{\mathrm{eff}}^{yy}}]\omega a_x/c$ neglected in the quasi-static approximation based on periodic electrostatic potentials. More accurate description of ϵ_{eff} should include spatial dispersion [43]. Development of an adequate theory of this phenomenon in plasmonic crystals is under way.

3. Perturbation theory of optical response of plasmonic nanostructures

In Section 2 we have described several theoretical approaches to calculating $\epsilon_{\mathrm{eff}} \approx \epsilon_{\mathrm{qs}}$ for sub-wavelength nanostructures. A much more challenging problem is attacked in this Section: computing the magnetic permeability $\mu_{\mathrm{eff}}(\omega)$. One of the intriguing results is that $\mu_{\mathrm{eff}}(\omega)$ can be strongly dependent on the propagation direction for low-symmetry structures such as the recently described metal strip pairs and SPOFs [20,27,44].

3.1. From electrostatics to optical magnetism

In this section, we present a sketch of a perturbation theory that uses electrostatic plasmon eigenfunctions, which are known to provide a complete orthogonal basis in

the appropriate linear space [29,41], as the starting point. Unlike earlier two-dimensional treatments [45], this theory is applicable to both two- and three-dimensional structures. In this section, calculations are presented for three-dimensional plasmonic crystals; expressions for two-dimensional crystals are derived by replacing the measure of integration $\mathrm{d}V \to a_z \mathrm{d}x\mathrm{d}y$, where a_z is an arbitrary "period" in the z-direction, which can be set to a unit length. The expansion parameter of this theory is the dimensionless retardation parameter $\eta = \omega a/c$. The goal of this Section is to obtain a self-consistent analytic expression for μ_{eff} of a periodic plasmonic nanostructure in the form of an eigenmode expansion.

In conventional atomic crystals, low-frequency magnetism stems mostly from internal and orbital magnetic moments of electrons. In dielectric structures, including plasmonic metamaterials, magnetism originates from polarization and conduction currents; total local current equals $\vec{j} = -\mathrm{i}\omega(\epsilon - 1)\vec{E}/4\pi$ where the local complex permittivity ϵ also contains conductivity. These currents determine both ϵ_{eff} and μ_{eff}; their contributions to these parameters can be determined unambiguously by splitting the total local current into "electric" and "magnetic" parts: $\vec{j} = \vec{j}_E + \vec{j}_M$. The electric dipole moment of a unit cell is defined as $\vec{p} = \int \mathrm{d}V \vec{P}_E$, where $\vec{P}_E = \mathrm{i}/\omega \vec{j}_E$; effective permittivity is defined by expression $p_i = V\left(\epsilon^{ij}_{\mathrm{eff}} - \delta^{ij}\right) E_{0j}/4\pi$, where V is the volume of a unit cell. Splitting of the local current into $\vec{j}_E$ and $\vec{j}_M$ becomes unambiguous, if we require that $\vec{j}_M$ do not contribute to the electric dipole moment $\vec{p}$, i.e. $\langle \vec{j}_M \rangle \equiv \int \mathrm{d}V \vec{j}_M = 0$. The effective magnetic permeability μ_{eff} is defined by a similar expression, $m_i = V\left(\mu^{ij}_{\mathrm{eff}} - \delta^{ij}\right) H_{0j}/4\pi$, in which the magnetic dipole moment is calculated as $\vec{m} = \int \mathrm{d}V \vec{M}$, where $\vec{M} = \frac{1}{2c}[\vec{r} \times \vec{j}_M]$ is the magnetic polarization density. Optical magnetism appears in the ω^2 order of this perturbation theory [20,32]. Since $\vec{j}_M$ already has one factor of ω, to determine μ_{eff} in the lowest order it suffices to calculate $\vec{E}$ with the first-order electromagnetic corrections.

To isolate the role of electrostatic resonances, it is convenient to decompose electric and magnetic fields into "incident" and "scattered", i.e. $\vec{E} = \vec{E}_{in} + \vec{E}_{\mathrm{sc}}$ and $\vec{H} = \vec{H}_{in} + \vec{H}_{\mathrm{sc}}$, such that $\vec{E}_{\mathrm{sc}}$ and $\vec{H}_{\mathrm{sc}}$ vanish in a homogeneous structure. To achieve this, we use the plane wave ansatz: $\vec{E}_{in} = \vec{E}_0 \mathrm{e}^{\mathrm{i}\vec{k}\cdot\vec{r}}$ and $\vec{H}_{in} = \vec{H}_0 \mathrm{e}^{\mathrm{i}\vec{k}\cdot\vec{r}}$. After the effective medium parameters ϵ_{eff} and μ_{eff} are expressed through $\vec{k}$, we use the dispersion relation of transverse waves in a homogenized medium: $k = \sqrt{\epsilon_{\mathrm{eff}}}\sqrt{\mu_{\mathrm{eff}}}\omega/c$ to determine $\epsilon_{\mathrm{eff}}(\omega)$ and $\mu_{\mathrm{eff}}(\omega)$. This calculation is reminiscent of the Maxwell Garnett (MG) effective medium theory, where individual particles to be homogenized are assumed to be immersed inside an effective medium with some unknown (and self-consistently determined) ϵ_{eff} and μ_{eff}. To simplify the calculation, we assume that $\vec{k} \parallel \hat{x}$, $\vec{E}_0 \parallel \hat{y}$ and $\vec{H}_0 \parallel \hat{z}$. Therefore, $\mu_{\mathrm{eff}} \equiv \mu^{zz}_{\mathrm{eff}}$. Additionally, because the incident fields satisfy Maxwell's equations in the homogenized medium, we have $\vec{H}_0 = Z_e^{-1}[\vec{n}_k \times \vec{E}_0]$, where $Z_e = \sqrt{\mu_{\mathrm{eff}}}/\sqrt{\epsilon_{\mathrm{eff}}}$ is effective impedance and $\vec{n}_k = \vec{k}/|\vec{k}|$ is the direction of the phase velocity.

Before proceeding to calculating the magnetic moment, note that the requirement $\langle \vec{j}_M \rangle = 0$ is satisfied with the following decomposition of currents: $\vec{j}_E = -\mathrm{i}\omega(\epsilon_{\mathrm{eff}} - 1)\vec{E}/(4\pi)$, $\vec{j}_M = -\mathrm{i}\omega(\epsilon - \epsilon_{\mathrm{eff}})\vec{E}/(4\pi)$, as long as ϵ_{eff} satisfies equality $\epsilon_{\mathrm{eff}} \int \mathrm{d}V \vec{E} = \int \mathrm{d}V \epsilon \vec{E}$. One can verify that this definition of ϵ_{eff} is the same as the one given by the total electric dipole moment of a unit cell, because $\langle \vec{j} \rangle = \langle \vec{j}_E \rangle$. Moreover, $\epsilon_{\mathrm{eff}} = \epsilon_{\mathrm{qs}} + O(\eta^2)$, where ϵ_{qs} is given by Eq. (17).

The scattered electric field $\vec{E}_{\mathrm{sc}}$ is decomposed into the potential and solenoidal parts, $\vec{E}_{\mathrm{sc}} = \vec{E}_{\mathrm{pot}} + \vec{E}_{\mathrm{sol}} = -\vec{\nabla}\Phi_{\mathrm{sc}} + \mathrm{i}k_0\vec{A}_{\mathrm{sc}}$, where $\vec{\nabla}\cdot\vec{A}_{\mathrm{sc}} = 0$ and $k_0 \equiv \omega/c$. Note that $\vec{A}_{\mathrm{sc}}$ is related to the scattered magnetic field: $\vec{H}_{\mathrm{sc}} = (\mu_{\mathrm{eff}} - 1)\vec{H}_{in} + \vec{\nabla} \times \vec{A}_{\mathrm{sc}}$. It can be demonstrated $\vec{A}_{\mathrm{sc}}$ is first order in η, making the contribution of $\vec{A}_{\mathrm{sc}}$ to $\vec{E}_{\mathrm{sc}}$ second order in η. Therefore, the lowest-order (η^2) expression for $\mu_{\mathrm{eff}} - 1$ can be found without directly computing $\vec{A}_{\mathrm{sc}}$ or magnetic fields.

The potential part of $\vec{E}_{\mathrm{sc}}$ is determined from $\vec{\nabla}\cdot\vec{D} = 0$, resulting in

$$\vec{\nabla}\epsilon\vec{E}_{\mathrm{pot}} = -\vec{\nabla}\epsilon\vec{E}_{in} - \vec{\nabla}\epsilon\vec{E}_{\mathrm{sol}} \equiv -\left(\vec{E}_{in} + \mathrm{i}k_0\vec{A}_{\mathrm{sc}}\right)\cdot\vec{\nabla}\epsilon, \quad (20)$$

where $k_0\vec{A}_{\mathrm{sc}}$ can be neglected to order η^2. For completeness, we note that $\vec{A}_{\mathrm{sc}}$ is computed, to the lowest order in η, as

$$-\nabla^2\vec{A}_{\mathrm{sc}} - \mathrm{i}k_0\epsilon\vec{\nabla}\Phi^{(0)}_{\mathrm{sc}} = \mathrm{i}k_0(\epsilon_{\mathrm{qs}} - \epsilon)\vec{E}_{in}. \quad (21)$$

Using the approach similar to the one taken in Ref. [45], Φ_{sc} is expanded as $\Phi_{\mathrm{sc}}(X,x) = \sum_n c_n(X)\phi_n(x)$, where ϕ_n are electrostatic eigenfunctions of the GEDE with periodic boundary conditions. Function $\Phi_{\mathrm{sc}}(X,x)$ is periodic in the "local" coordinate x and depends upon the "macroscopic" coordinate X as the macroscopic fields, i.e. $\propto \mathrm{e}^{\mathrm{i}kX}$ under assumptions of our ansatz. This eigenmode expansion is justified because the full set of $\phi_n(x)$ functions is a complete basis in the space of periodic solutions to Laplace equation [46]. The coupling coefficient c_n between $\vec{E}_{in}(X,x) = \vec{E}_0\mathrm{e}^{\mathrm{i}kX}\mathrm{e}^{\mathrm{i}kx}$ and the nth plasmon eigenmode are found by applying the EE approach described in Section 2.3 to Eq. (20):

$$c_n = -\frac{s_n}{s(\omega) - s_n}\frac{\int(\vec{\nabla}\phi_n)\vec{E}_{in}\theta\mathrm{d}V}{\int(\nabla\phi_n)^2\theta\mathrm{d}V} + O(\eta^2). \quad (22)$$

Coefficients $c_n(X) = c_n(0)\mathrm{e}^{\mathrm{i}kX}$ absorb the phase shift per cell; it is sufficient to calculate them in the very first cell, i.e. at $X = 0$. Expanding the plane wave $\vec{E}_{in} = \vec{E}_0\mathrm{e}^{\mathrm{i}kx}$ in the powers of k up to the first order, we obtain $c_n = c_n^{(0)} + c_n^{(1)}$, where

$$c_n^{(m)} = -\frac{1}{m!}(\mathrm{i}\sqrt{\epsilon_{\mathrm{eff}}}\sqrt{\mu_{\mathrm{eff}}}k_0)^m\frac{s_n}{s(\omega) - s_n}\vec{E}_0 \times \frac{\int(\vec{\nabla}\phi_n)x^m\theta\mathrm{d}V}{\int(\nabla\phi_n)^2\theta\mathrm{d}V}, \quad m = 0, 1. \quad (23)$$

The scattered field $\vec{E}_{\mathrm{sc}}$ is now used to calculate m_z and, consequently, μ_{eff}. For simplicity, we assume that the structure has a center of inversion that coincides with the center of mass of a unit cell. Choosing it as the origin of coordinate system, we have $\langle \vec{r}\theta \rangle = 0$ and $\langle \vec{r} \rangle = 0$. This eliminates the term $\int(\epsilon - 1)\vec{r} \times \vec{E}_0\mathrm{d}V$, and also guarantees that the

dipole eigenmodes ϕ_n in $\Phi_{\rm sc}$ excited by uniform field $\vec{E}_0$ do not carry magnetic moment, as explained below. Under these assumptions, $\mu_{\rm eff}-1\propto k_0^2$. The currents excited directly by $\vec{E}_{in}$ produce a diamagnetic contribution to $\mu_{\rm eff}$:

$$\Delta\mu_{\rm diam}=\frac{k_0^2\mu_{\rm eff}}{2V}\left[(\epsilon_d-\epsilon_{\rm eff})\int x^2{\rm d}V-\frac{\epsilon_d}{s}\int x^2\theta{\rm d}V\right], \quad (24)$$

where V is the volume of a unit cell. Quasistatic currents due to $\vec{E}_{\rm sc}\approx-\vec{\nabla}\Phi_{\rm sc}$ give the plasmon resonance part of the magnetic permeability:

$$\Delta\mu_{\rm plasm}=-k_0^2\epsilon_d\mu_{\rm eff}\sum_n\frac{F_n^{zz}}{s(\omega)-s_n}+k_0^2\epsilon_d\mu_{\rm eff}\frac{1}{s}\sum_n K_n^{zz}, \quad (25)$$

where

$$F_n^{zz}=K_n^{zz}+(\epsilon_{\rm eff}/\epsilon_d-1)G_n^{zz} \quad (26)$$

is the magnetic strength of nth resonance,

$$K_n^{zz}=\frac{1}{2}\frac{\int\left(x\frac{\partial\phi_n}{\partial y}\theta\right){\rm d}V\int(\vec{e}_z\cdot[\vec{r}\times\nabla\phi_n]\theta)\,{\rm d}V}{V\int(\nabla\phi_n)^2\theta{\rm d}V}$$

$$\text{and}\quad G_n^{zz}=\frac{1}{2}\frac{\int\left(x\frac{\partial\phi_n}{\partial y}\theta\right){\rm d}V\int(\vec{e}_z\cdot[\vec{r}\times\nabla\phi_n])\,{\rm d}V}{V\int(\nabla\phi_n)^2\theta{\rm d}V}.$$

Finally, permeability is determined from $\mu_{\rm eff}-1=\Delta\mu_{\rm diam}+\Delta\mu_{\rm plasm}$:

$$1-\frac{1}{\mu_{\rm eff}^{zz}}=\mu_d^{zz}-k_0^2\epsilon_d\frac{F_0^{zz}}{s(\omega)}-k_0^2\epsilon_d\sum_n\frac{F_n^{zz}}{s(\omega)-s_n}, \quad (27)$$

where $\mu_d^{zz}=k_0^2(\epsilon_d-\epsilon_{\rm eff})\langle\frac{x^2}{2}\rangle$ and $F_0^{zz}=\left(\langle\frac{x^2}{2}\theta\rangle-\sum_n K_n^{zz}\right)$. Here the sum over electrostatic resonances possessing a finite magnetic moment $\int(\vec{e}_z\cdot[\vec{r}\times(\epsilon-\epsilon_{\rm eff})\nabla\phi_n])\,{\rm d}V$ represents the resonant contribution to magnetic permeability, while the term proportional to F_0^{zz} represents the expulsion of the magnetic field from the plasmonic inclusion. Eq. (27) can be generalized for an arbitrary propagation direction $\vec{k}$.

Eq. (27) should be used with caution at very large negative dielectric contrasts, i.e. when $0<s(\omega)\ll 1$. In this regime, plasmonic inclusions behave as good conductors. Expulsion of magnetic field from plasmonic phase becomes so strong, that, in fact, scattered magnetic field $\vec{H}_{\rm sc}$ is nearly equal in magnitude (and opposite in sign) to the incident magnetic field $\vec{H}_{in}$. Present theory treats $\vec{H}_{\rm sc}$ as perturbation and is therefore inaccurate in this regime. This limitation manifests in Eq. (27) as an unphysical pole at $s=0$. Its origin can be seen from Mie theory of a dielectric sphere.

For a sphere, all plasmon resonances have zero magnetic strength, $F_n^{zz}=0$, and $F_0^{zz}=\langle\frac{x^2}{2}\theta\rangle=\frac{1}{30}4\pi R^5/V$, where $V\gg R^3$ is the volume of a very large domain in which a sphere is contained. Our formula (27) gives $1-1/\mu_{\rm eff}\approx\mu_{\rm eff}-1\equiv 4\pi\chi_M/V=-k_0^2F_0^{zz}/s(\omega)$, where χ_M is the magnetic polarizability of a plasmonic sphere. For $\epsilon_d=1$ we obtain $\chi_M/R^3=\frac{1}{30}(\epsilon-1)(k_0R)^2$. The exact Mie result for the magnetic polarizability of a sphere is

$$\frac{\chi_M}{R^3}=\frac{3{\rm i}e^{-{\rm i}\eta}}{2\eta^3}\times\frac{\cos\eta\sin m\eta-\frac{1}{m}\cos m\eta\sin\eta-(1-\frac{1}{m^2})\sin\eta\sin m\eta/\eta}{\sin m\eta+\frac{\rm i}{m}\cos m\eta+{\rm i}(1-\frac{1}{m^2})\sin m\eta/\eta}, \quad (28)$$

where $\eta=k_0R$ and $m^2=\epsilon(\omega)$. Eq. (28) can be simplified in two limiting cases: (a) $\eta\ll 1$ and arbitrary m, and (b) $|m^2|\gg 1$ and arbitrary η. The former expansion results in

$$\chi_M^{(a)}/R^3=\frac{1}{30}(m^2-1)\eta^2+O(\eta^4), \quad (29)$$

in agreement with Eq. (27). The latter expansion results in

$$\frac{\chi_M^{(b)}}{R^3}=\frac{3{\rm i}e^{-{\rm i}\eta}(\eta\cos\eta-\sin\eta)}{2\eta^3(\eta+{\rm i})}. \quad (30)$$

For $k_0R\to 0$ we recover the textbook result for magnetization of a perfectly conducting small sphere: $\chi_M^{(b)}=-1/2R^3$. Therefore, $\chi_M^{(a)}$ overestimates the magnetic polarizability of the sphere whenever $\eta\ll 1$ but $|m\eta|>1$. The quasi-static theory developed here suffers from the same limitation. Nevertheless, the analytic expression for the effective magnetic permeability $\mu_{\rm eff}(\omega)$ of a plasmonic nanostructure given by Eq. (27) answers several fundamental questions outlined below.

3.1.1. Which plasmon resonances are magnetic?

It has been observed earlier [20,23] that in the structures with a sufficiently high spatial symmetry only some plasmon resonances may have a non-vanishing magnetic strength given by Eq. (26). Such eigenmodes are sometimes referred to as *magnetic plasmon resonances* (MPR) [32]. For example, if the structure has an inversion center, its electrostatic eigenfunctions ϕ_n can be either even or odd with respect to spatial inversion. It follows from the definitions of f_n^{ij} and F_n^{zz} that even modes have a vanishing electric strength while the odd modes have a vanishing magnetic strength. If inversion center is the only non-trivial element of symmetry, i.e. the structure's symmetry group is C_i, all even modes are magnetic resonances ($F_n\neq 0$) and odd modes — electric resonances ($f_n\neq 0$). For example, the electrostatic resonance of the SPOF structure shown in Fig. 2(c) has a finite magnetic strength proportional to η^2.

In structures with higher symmetries, electric and magnetic eigenmodes can be identified by their irreducible representation. It can be shown that electric strength f_n^{xx} may only be non-zero if the corresponding potential ϕ_n transforms under the same representation as the coordinate x (and similarly for f_n^{yy} and f_n^{zz}). For the magnetic strength F_n^{zz} to be non-vanishing, the potential ϕ_n must transform as an operator of rotation around z-axis (R_z), which is a component of a pseudovector. Standard character tables of the point groups of symmetry [47] provide the information necessary for assigning magnetic or electric dipole activity to various resonances.

In the structures without an inversion center, some eigenmodes may transform as both x and R_z, meaning that

they contribute to both $\epsilon_{\rm eff}^{xx}$ and $\mu_{\rm eff}^{zz}$. In addition, they provide magneto-electric coupling between E_y and H_z. Whenever such modes exist, the structure is termed *bi-anisotropic*: it may not be described with $\epsilon_{\rm eff}(\omega)$ and $\mu_{\rm eff}(\omega)$ tensors alone [48]. SRR and SR are examples of such bi-anisotropic structures [49], and their electrostatic resonances shown in Fig. 2(a), (b) contribute to both μ^{zz} and $\epsilon_{\rm qs}^{xx}$.

3.1.2. Does the magnetic permeability depend on the propagation direction?

The magnetic strength F_n^{zz}, given by Eq. (26), may depend on the orientation of the wave vector $\vec{k}$ (or electric field $\vec{E}_0$) in the plane orthogonal to $\vec{H}_0$. Consequently, magnetic permeability $\mu_{\rm eff}^{zz}$ near an MPR can be anisotropic. This happens because the magnetic strength is a product of two factors: (i) coupling of the incident plane wave to a plasmon mode, and (ii) magnetic moment contained in the excited mode. While the latter is independent of the direction of $\vec{k}$ or $\vec{E}_0$, the former coupling is determined by the inhomogeneity of the electric field $\vec{E}_0 e^{i\vec{k}\cdot\vec{r}}$ and, therefore, depends upon the orientation of the orthogonal pair $(\vec{k}, \vec{E}_0)$. In other words, the components of the $\mu_{\rm eff}$ tensor of a plasmonic metamaterial are in general dependent on the propagation direction $\vec{k}/k$.

We use a pair of plasmonic strips (SPOF without the film) to illustrate the anisotropy of scalar $\mu_{\rm eff}$ in optical metamaterials. This structure has attracted a great deal of attention as a magnetic component of NIMs [20,44]. Its two-dimensional point group of symmetry is C_{2v}; electric plasmon resonances in this structure correspond to dipole-like eigenpotentials ϕ_n, and magnetic resonances are electric quadrupoles [20]. Quasi-static values of the effective permeability from Eq. (27) (labeled as $\mu_{\rm qs}$) are compared with those (labeled as $\mu_{\rm em}$) extracted from the single-layer electromagnetic scattering simulations. The two illumination geometries and the results are shown in Fig. 4. Unit cell dimensions are given in the caption to Fig. 4. Both quasistatic and electromagnetic results plotted in Fig. 4 demonstrate that the strength the magnetic plasmon resonance excitation depends strongly upon the direction of the wave vector $\vec{k}$ of the incident wave. Maximum deviation of $\mu_{\rm eff}$ from unity is an order of magnitude larger when $\vec{k}$ is perpendicular to the strips. The high degree of anisotropy of $\mu_{\rm eff}$ is related to the relatively low symmetry group (C_{2v}) of the two plasmonic strips.

For plasmonic nanostructures with the higher degree of symmetry (C_{3v}, C_{4v}, and C_{6v}) the anisotropy of $\mu_{\rm eff}^{zz}$ may disappear. For such structures it can be shown that the coupling coefficients in F_n^{zz} for $\vec{k}\|\hat{x}$ and $\vec{k}\|\hat{y}$ are equal in magnitude but differ in sign: $\int x\frac{\partial\phi_n}{\partial y}\theta {\rm d}V = -\int y\frac{\partial\phi_n}{\partial x}\theta {\rm d}V$. Therefore, $\int x\frac{\partial\phi_n}{\partial y}\theta {\rm d}V = \frac{1}{2}\int\left(x\frac{\partial\phi_n}{\partial y} - y\frac{\partial\phi_n}{\partial x}\right)\theta {\rm d}V$, and the magnetic strength F_n^{zz} as well as other parameters (μ_d^{zz} and F_0^{zz}) become isotropic. Thus, for sufficiently symmetric crystals it is possible to introduce an isotropic $\mu_{\rm eff}$, independent of the direction of applied electric field. A two-dimensional example of a plasmonic metamaterial with isotropic scalar $\mu_{\rm eff}$ is a square array of plasmonic nanorods shown earlier [22,23,50] to exhibit an isotropic negative refractive index.

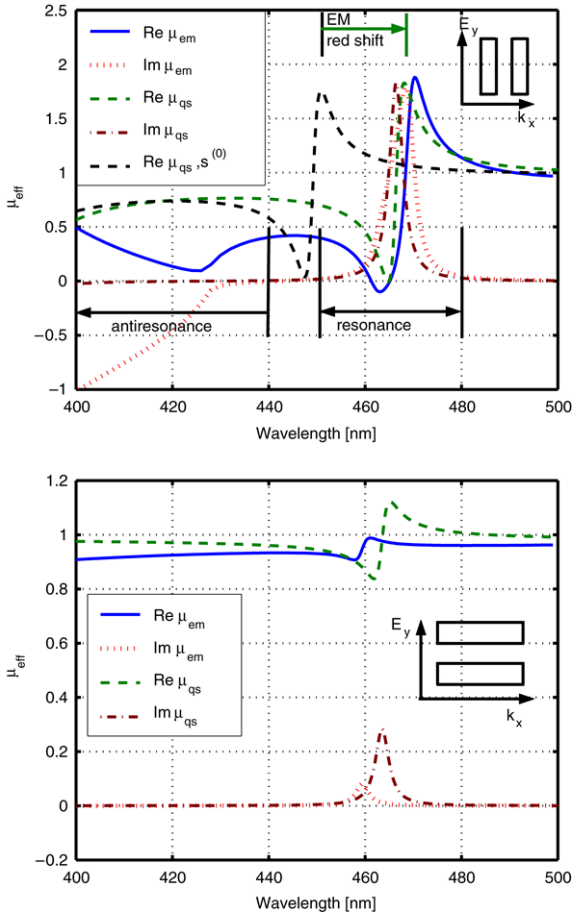

Fig. 4. (Color online) Effective magnetic permeability $\mu_{\rm eff}^{zz}$ of the strip pair structure calculated using two methods: electromagnetic scattering through a single layer (solid and dotted curves), and the quasi-static Eq. (27) (dashed and dash-dotted). Green dashed curve incorporates the retardation frequency shift given by Eq. (32). Black dashed curve is not corrected by the retardation frequency shift. Orientation of the strips and the incident electric field are shown in the insets. Structure parameters: periods $a_x = a_y = 100$ nm, strip width: $w = 50$ nm, strip thickness $t_s = 15$ nm, strip separation in the pair: $h = 15$ nm; Strips are assumed to be made of silver and embedded in vacuum ($\epsilon_d = 1$).

3.2. Electromagnetic red shifts of plasmonic resonances

Eq. (27) predicts that the frequency of magnetic plasmon resonance ω_n, determined from $s(\omega_n) = s_n$, is the frequency of *magnetic cut-off*, $\mu_{\rm eff} = 0$. From Fig. 4(a) we observe that the frequency of the magnetic cut-off determined from electromagnetic simulations (solid curve) is red-shifted with respect to the frequency of corresponding electrostatic resonance (black dashed curve). It can also be seen from Fig. 3 that electric dipole resonances in FEFD simulations are red-shifted with respect to their electrostatic positions. Both shifts can be explained as the retardation-induced corrections to the positions of the purely electrostatic plasmon resonances [33].

These frequency shifts are always red and can be understood physically as follows. Quasi-static currents associated with electric fields of electrostatic resonances induce magnetic fields via Ampere's law. These magnetic fields generate secondary electric fields according to the Faraday's law. The latter contribute to the Poisson equation $\vec{\nabla}\cdot\epsilon\vec{E} = 0$, causing shifts

in electrostatic eigenvalues. While such frequency shifts have been calculated earlier for isolated plasmonic nanoparticles, they have never been calculated for periodic plasmonic metamaterials.

Retardation shifts are computed using the perturbation theory developed in Section 3. To the lowest order in η and in the close vicinity of the nth plasmonic resonance (i.e., at $s \approx s_n^{(0)}$, where $s_n^{(0)}$ is the purely electrostatic eigenvalue of the Eq. (15)), the vector potential induced by the nth electrostatic resonance is found from Eq. (21): $\vec{A}_{\rm sc}^{(1)}(\vec{r}) = ik_0 \int dV' G(\vec{r} - \vec{r}')\epsilon(\vec{r}')\nabla\phi_n(\vec{r}')$, where $\epsilon \approx \epsilon_d \left(1 - \frac{1}{s_n^{(0)}}\theta\right)$, and $G(\vec{r} - \vec{r}')$ is the modified Green's function of Poisson equation with periodic boundary conditions originally calculated [51] in the context of the solid state physics. Thus computed vector potential $\vec{A}_{\rm sc}^{(1)}$ contributes to Poisson equation:

$$\vec{\nabla}\theta\vec{\nabla}\Phi + k_0^2\epsilon_d\vec{\nabla}\theta \cdot \int dV' G(r, r') \left(1 - \frac{1}{s_n^{(0)}}\theta\right) \vec{\nabla}\Phi = s_n \nabla^2 \Phi. \quad (31)$$

This is a generalized linear eigenvalue problem with integro-differential operator. Treating the integral term as a perturbation, corrections to electrostatic eigenvalues $s_n^{(0)}$ can be shown to be:

$$s_n^{(2)} = k_0^2\epsilon_d s_n^{(0)} \oint dS\phi_n(r)\vec{n} \times \int G(\vec{r} - \vec{r}') \left(1 - \frac{1}{s_n^{(0)}}\theta(\vec{r}')\right) \vec{\nabla}\phi_n(\vec{r}')dV' \times \left(\int |\nabla\phi_n|^2\theta dV\right)^{-1}, \quad (32)$$

where $\oint dS$ is a surface integral over a closed surface S of the plasmonic inclusion (which reduces to a contour integral for 2D crystals). The renormalized s_n is calculated as $s_n = s_n^{(0)} + s_n^{(2)}$. Volume integral in Eq. (32) can be reduced to a surface integration over the surface S by introducing an auxiliary vector $\vec{a}(\vec{r}, \vec{r}') = -\vec{\nabla} \int G(\vec{r} - \vec{r}'')G(\vec{r}'' - \vec{r}')dV''$:

$$s_n^{(2)} = k_0^2\epsilon_d \oint dS\phi_n(\vec{r})\vec{n} \cdot \oint dS'\vec{a}(\vec{r}, \vec{r}') \times [\vec{n}' \times \nabla\phi_n(\vec{r}')] \times \left(\oint \phi_n \frac{\partial\phi_n}{\partial n} dS\right)^{-1}, \quad (33)$$

where the normal derivative $\partial\phi_n/\partial n$ is evaluated on the plasmonic side of surface S. A particular case of this formula has been previously reported for isolated three-dimensional particles [33].

Despite substantial progress in calculations of periodic Green's functions [51], closed-form expressions for double- or triple-periodic G in two or three dimensions are not known. However, there exists one simple yet exact result for a 2D Green's function in the limit $a_y \gg a_x$ [51]:

$$G_2(\vec{r} - \vec{r}') = \frac{1}{2a_x}\left(\frac{(y - y')^2}{a_y} - |y - y'| + \frac{a_y}{6}\right) - \frac{1}{4\pi}\ln[1 - 2e^{-2\pi|y-y'|/a_x}\cos(2\pi|x - x'|/a_x) + e^{-4\pi|y-y'|/a_x}]. \quad (34)$$

The function (34) is periodic only in the x-direction. It is therefore applicable only for $|y - y'| \ll a_y$, i.e. when plasmonic inclusions are much thinner in the y-direction than the period ($w_y \ll a_y$). For periodic metamaterials based on "current loops" (strip pairs, horse shoes, etc.), interaction between consecutive layers of resonators is usually insignificant, and the function (34) provides reasonable approximation. When the condition $w_x \ll a_x$ is satisfied, one can use expression (34) with interchanged variables $x \leftrightarrow y$, $a_x \leftrightarrow a_y$. When both dimensions are small, $w_{x,y} \ll a_{x,y}$, a symmetrized (in x, y) version of Eq. (34) is used.

Retardation frequency shifts of selected electric and magnetic resonances are illustrated on Figs. 3 and 4, respectively. Frequency shifts are calculated using Eq. (32) with the Green's function given by Eq. (34). It is apparent that the quasi-static Eqs. (17) and (27) with frequency corrections corresponding to $s_n = s_n^{(0)} + s_n^{(2)}$ (green dashed curves on Figs. 3 and 4) are in much better agreement with the electromagnetic $\epsilon_{\rm eff}$ and $\mu_{\rm eff}$ than the unperturbed electrostatic eigenvalues $s_n^{(0)}$ (black dashed curves). In subsequent publications we will show analytically how these eigenvalue corrections appear in the resonant denominators $(s_n - s)$ of the driven problem.

4. Summary

In this review we have discussed several physics issues important for designing sub-wavelength plasmonic metamaterials in the optical part of the spectrum. Several techniques for calculating the effective dielectric permittivity $\epsilon_{\rm eff} \approx \epsilon_{\rm qs}$ in the quasi-static limit are discussed. We have presented a sketch of a homogenization theory that encompasses both electric and magnetic response of plasmonic nanostructures. As suggested by electrostatic nature of plasmon resonances, the theory starts from the electrostatic description and takes retardation and magnetic phenomena into account perturbatively. Formulas for the frequencies and strengths of all electric and magnetic resonances are universally applicable to any periodic metallo-dielectric nanostructures operating in the plasmonic regime. The theory is supported by first-principle electromagnetic simulations. Our results demonstrate that in 2D plasmonic crystals without rotational symmetry, such as strip pair arrays, scalar magnetic permeability $\mu_{\rm eff}^{zz}$ depends on the orientation of electric field (or the wavenumber).

Acknowledgements

This work is supported by the ARO MURI W911NF-04-01-0203, AFOSR MURI FA9550-06-01-0279, the DARPA contract HR0011-05-C-0068, and by the NSF's NIRT 0709323.

References

[1] V.G. Veselago, The electrodynamics of substances with simultaneously negative values of ϵ and μ, Soviet Phys. – Uspekhi 10 (1968) 509.

[2] J.B. Pendry, Phys. Rev. Lett. 85 (2000) 3966.
[3] Y. Horii, C. Caloz, T. Itoh, IEEE Trans. Microwave Theory Tech. 53 (2005) 1527.
[4] A. Alu, N. Engheta, IEEE Trans. Microwave Theory Tech. 52 (2004) 199.
[5] R.W. Ziolkowski, A. Erentok, Metamaterial-based efficient electrically small antennas, IEEE Trans. Antennas Propag. 54 (2006) 2113.
[6] J.B. Pendry, D. Schurig, D.R. Smith, Controlling electromagnetic fields, Science 312 (2006) 1780.
[7] U. Leonhardt, Optical conformal mapping, Science 312 (2006) 1777.
[8] D. Schurig, J.J. Mock, B.J. Justice, S.A. Cummer, J.B. Pendry, A.F. Starr, D.R. Smith, Metamaterial electromagnetic cloak at microwave frequencies, Science 314 (2006) 977.
[9] D.R. Smith, W.J. Padilla, D.C. Vier, S.C. Nemat-Nasser, S. Schultz, Phys. Rev. Lett. 84 (2000) 4184.
[10] J.B. Pendry, A.J. Holden, D.J. Robbins, W.J. Stewart, IEEE Trans. Microwave Theory Tech. 47 (1999) 2075.
[11] J.B. Pendry, A.J. Holden, W.J. Stewart, I. Youngs, Phys. Rev. Lett. 76 (1996) 4773.
[12] E. Yablonovich, Phys. Rev. Lett. 58 (1987) 2059.
[13] S. John, Phys. Rev. Lett. 58 (1987) 2486.
[14] S. Zhang, W. Fan, N.C. Panoiu, K.J. Malloy, R.M. Osgood, S.R.J. Brueck, Experimental demonstration of near-infrared negative-index metamaterials, Phys. Rev. Lett. 95 (2005) 137404.
[15] G. Dolling, C. Enkrich, M. Wegener, J.F. Zhou, C.M. Soukoulis, S. Linden, Opt. Lett. 30 (2005) 3198.
[16] V.M. Shalaev, W. Cai, U.K. Chettiar, H.-K. Yuan, A.K. Sarychev, V.P. Drachev, A.V. Kildishev, Negative index of refraction in optical metamaterials, Opt. Lett. 30 (2005) 3356.
[17] G. Dolling, C. Enkrich, M. Wegener, C.M. Soukoulis, S. Linden, Simultaneous negative phase and group velocity of light in a metamaterial, Science 312 (2006) 892.
[18] A.N. Grigorenko, A.K. Geim, H.F. Gleeson, Y. Zhang, A.A. Firsov, I.Y. Khrushchev, J. Petrovic, Nanofabricated media with negative permeability at visible frequencies, Nature 438 (2005) 335.
[19] W. Cai, U.K. Chettiar, H.-K. Yuan, V.C. de Silva, A.V. Kildishev, V.P. Drachev, V.M. Shalaev, Metamagnetics with rainbow colors, Opt. Exp. 15 (2007) 3333.
[20] G. Shvets, Y.A. Urzhumov, Negative index meta-materials based on two-dimensional metallic structures, J. Opt. A: Pure Appl. Opt. 8 (2006) S122.
[21] G. Shvets, Phys. Rev. B. 338 (2003) 035109.
[22] G. Shvets, Y. Urzhumov, Engineering the electromagnetic properties of periodic nanostructures using electrostatic resonances, Phys. Rev. Lett. 93 (2004) 243902.
[23] G. Shvets, Y. Urzhumov, Electric and magnetic properties of sub-wavelength plasmonic crystals, J. Opt. A: Pure Appl. Opt. 7 (2005) S23–S31.
[24] D.R. Smith, S. Schultz, P. Markos, C.M. Soukoulis, Phys. Rev. B 65 (2002) 195104.
[25] P. Markos, C.M. Soukoulis, Opt. Exp. 11 (2003) 649.
[26] T. Koschny, P. Markos, D.R. Smith, C.M. Soukoulis, Resonant and antiresonant frequency dependence of the effective parameters of metamaterials, Phys. Rev. E 68 (2003) 065602.
[27] V. Lomakin, Y. Fainman, Y. Urzhumov, G. Shvets, Doubly negative metamaterials in the near infrared and visible regimes based on thin nanocomposites, Opt. Exp. 14 (2006) 11164.
[28] M.I. Stockman, S.V. Faleev, D.J. Bergman, Phys. Rev. Lett. 87 (2001) 167401.
[29] M.I. Stockman, D.J. Bergman, T. Kobayashi, Coherent control of nanoscale localization of ultrafast optical excitation in nanosystems, Phys. Rev. B 69 (2004) 054202.
[30] V.A. Podolskiy, A.K. Sarychev, V.M. Shalaev, Plasmon modes and negative refraction in metal nanowire composites, Opt. Exp. 11 (2003) 735.
[31] A. Alu, A. Salandrino, N. Engheta, Negative effective permeability and left-handed materials at optical frequencies, Opt. Exp. 14 (2006) 1557.
[32] A.K. Sarychev, G. Shvets, V.M. Shalaev, Magnetic plasmon resonance, Phys. Rev. E 73 (2006) 036609.
[33] I.D. Mayergoyz, D.R. Fredkin, Z. Zhang, Phys. Rev. B 72 (2005) 155412.
[34] A.B. Comsol, M.A. Burlington, COMSOL Multiphysics User's Guide, Version 3.3, August 2006.
[35] E.D. Palik (Ed.), Handbook of Optical Constants of Solids, Vol. 1, Academic Press, Orlando, FL, 1985.
[36] N. Engheta, A. Salandrino, A. Alu, Circuit elements at optical frequencies: Nanoinductors, nanocapacitors, and nanoresistors, Phys. Rev. Lett. 95 (2005) 095504.
[37] S. Linden, C. Enkrich, M. Wegener, J. Zhou, T. Koschny, C.M. Soukoulis, Magnetic response of metamaterials at 100 terahertz, Science 306 (2004) 1351.
[38] D.R. Smith, J.B. Pendry, Homogenization of metamaterials by field averaging, J. Opt. Soc. Am. B 23 (2006) 391.
[39] G.W. Milton, The Theory of Composites, Cambridge University Press, 2002.
[40] V.V. Zhikov, Homogenization of Differential Operators and Integral Functionals, Springer-Verlag, New York, Berlin, 1994.
[41] D. Bergman, D. Stroud, Solid State Phys. 46 (1992) 147.
[42] D.R. Fredkin, I.D. Mayergoyz, Phys. Rev. Lett. 91 (2003) 253902.
[43] V.M. Agranovich, Y.N. Gartstein, Phys. – Uspekhi 49 (2006) 1029.
[44] U.K. Chettiar, A.V. Kildishev, T.A. Klar, V.M. Shalaev, Negative index metamaterial combining magnetic resonators with metal films, Opt. Exp. 14 (2006) 7872.
[45] D. Felbacq, G. Bouchitté, Theory of mesoscopic magnetism in photonic crystals, Phys. Rev. Lett. 94 (2005) 183902.
[46] D. Bergman, K.-J. Dunn, Phys. Rev. B 45 (1992) 13262.
[47] G.F. Koster, J.O. Dimmock, R.G. Wheeler, H. Statz, Properties of the Thirty-Two Point Groups, MIT Press, Cambridge, Mass, 1963.
[48] O.N. Singh, A. Lakhtakia (Eds.), Electromagnetic Waves in Unconventional Materials and Structures, John Wiley, New York, 2000.
[49] R. Marques, F. Medina, R. Rafii-El-Idrissi, Role of bianisotropy in negative permeability and left-handed metamaterials, Phys. Rev. B 65 (2002) 144440.
[50] M. Davanco, Y. Urzhumov, G. Shvets, The complex Bloch bands of a 2d plasmonic crystal displaying isotropic negative refraction, Opt. Exp. 15 (2007) 9681.
[51] S.L. Marshall, A periodic Green function for calculation of Coulomb lattice potentials, J. Phys.: Condens. Mat. 12 (2000) 4575.